J. Fluid Mech. (1967), *vol.* 27, *part* 1, *pp.* 1–28
Printed in Great Britain

Two supercavitating hydrofoils near a free surface

By T. GREEN† AND R. L. STREET
Stanford University

(Received 9 September 1965 and in revised form 7 November 1966)

A two-dimensional, incompressible, irrotational, linearized flow model is employed in this analysis of two supercavitating, flat-plate hydrofoils in the presence of a free surface. The cavities are taken to have finite lengths, and gravity is neglected. The ensuing boundary-value problem is converted, by means of conformal mapping, to a mixed-boundary-value problem for the complex velocity in the upper half-plane. This altered problem is solved by use of the methods of thin-aerofoil theory and the solution involves digital-computer evaluation of a large number of incomplete elliptic integrals of the first and third kinds. Typical results are presented in graphs, and the results of the present work are compared with Yim's (1964) theory for a single supercavitating body near a free surface.

1. Introduction

The past decade has witnessed many advances in the analytical treatment of cavity flows occurring with the use of high-speed underwater vehicles (Tulin 1964). In large part, the problems considered have been restricted to variously shaped single bodies that are a great distance from any free surface other than the cavity streamlines. It is common knowledge, however, that many practical cavitation problems include two cavitating bodies that operate in close proximity to a free surface. As an example, any high-speed hydrofoil vessel has at least two supporting foils that may be in a supercavitating state.

Free-surface effects on single supercavitating hydrofoils have been treated by a limited number of authors, and these works have culminated in Yim's (1964) linearized treatment of a flat-plate hydrofoil with a finite cavity that is near the water surface. The only work dealing with two hydrofoils was presented by Hsieh (1964), who analysed two foils with infinitely long cavities near the water surface.

The present analysis may be regarded as the logical continuation of both of the above-mentioned contributions. Two flat-plate hydrofoils were placed near a free surface, and the cavities were taken to be finite in length (i.e. the cavitation number was non-zero). Tulin's linearized double-spiral-vortex model was used (Tulin 1964). Figure 1 depicts the physical plane for this model in the case under consideration. Each cavity is assumed to close on a pair of small double-spiral vortices. They lead, in turn, to a thin wake (open at infinity), on the boundary of which the flow speed and pressure are constant. The wake and the vortices are suggestive of the highly turbulent and dissipative flow present in a real flow. The

† Now at the United States Naval Postgraduate School, Monterey, California.

vortices actually arise mathematically from the jump in the flow speed between the cavity surface and the wake. Upon linearization, this model provides known conditions on the complex velocity in the regions of the trailing wakes (as well as on the other pertinent boundaries), and gives the sharp pressure increase that is known to accompany cavity–wake transitions. The analytical work is quite straightforward, but the final solution must be carried out on a high-speed digital computer.

2. Problem formulation and solution

Two unit-length flat-plate hydrofoils are inclined at angles of attack γ_1 and γ_2 to the oncoming free stream (figures 1 and 2). The origin of the Cartesian co-ordinate frame is fixed at the leading edge of the upper foil, which is a vertical distance H_1 from the undisturbed free surface. The lower foil is a distance H_2 below the upper. Either of the two foils may be upstream of the other, depending on the

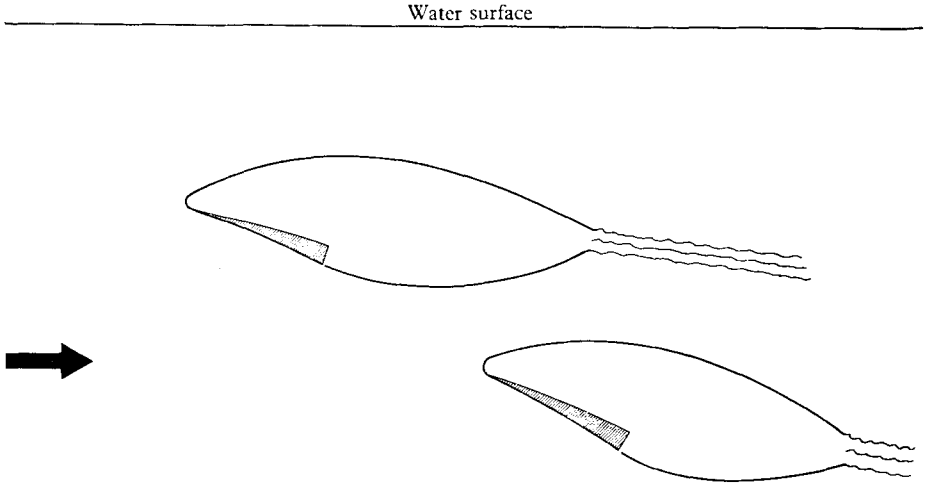

FIGURE 1. Two supercavitating hydrofoils near a free surface.

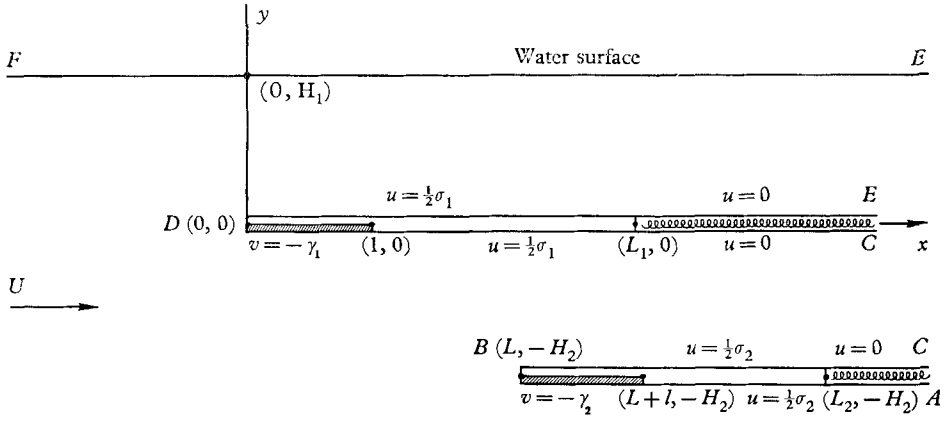

FIGURE 2. The linearized flat-plate problem.

sign of the tip-to-tip distance L. The upper and lower body–cavity systems are of lengths L_1 and $L_2 - L$, respectively.

The two-dimensional fluid-velocity vector $\mathbf{q}$ is normalized on U, the uniform velocity at infinity, so that $\mathbf{q} = U(1+u, v)$. Thus, u and v are the horizontal and vertical perturbation velocities that are superposed on a uniform flow. These quantities are assumed to be small: $u, v \ll 1$.

The flow is assumed to be inviscid, incompressible, and irrotational. Under these conditions, the complex velocity $w(x, y) = u(x, y) - iv(x, y)$ is known to be an analytic function of the complex variable $z = x + iy$. After gravity effects are neglected and second-order terms in u and v are dropped, the Bernoulli equation takes the form

$$p + \rho U^2 u = \Pi, \tag{1}$$

where p is the fluid static pressure, ρ the fluid density, and Π the pressure at an infinite distance from the plates. The essential dimensionless parameter is the cavitation number

$$\sigma_i = \frac{\Pi - p_i}{\frac{1}{2}\rho U^2},$$

where p_i is the pressure in the cavity behind the relevant plate. In terms of the cavitation number, the linearized Bernoulli equation (1) applied to a cavity streamline then becomes

$$\sigma_i = 2u_i, \tag{2}$$

where u_i is the horizontal perturbation velocity on the ith-cavity streamlines.

The usual tangency condition must be met on the undersides of the plates, and specified pressures must exist on the free water surface, on the cavity streamlines, and in the trailing wakes. The Tulin double-spiral-vortex flow model is used (Tulin 1964), so that the pressure in each wake (as well as on the water surface) is Π. The cavity pressures are independent parameters in the problem and will be related through the cavitation numbers to the cavity lengths and the lift coefficients.

In accordance with the order of approximation implied in linearized theory, the boundary conditions are transferred to the appropriate horizontal line, as illustrated in figure 2. When the linearized Bernoulli equation (2) is employed to relate pressures and velocities, these conditions become

$$\left.\begin{aligned} u &= 0 \text{ on the free water surface and in both wakes,} \\ u &= \tfrac{1}{2}\sigma_1 \text{ on the upper-foil-cavity streamlines,} \\ u &= \tfrac{1}{2}\sigma_2 \text{ on the lower-foil-cavity streamlines,} \\ v &= -\gamma_1 \text{ on the wetted surface of the upper foil,} \\ v &= -\gamma_2 \text{ on the wetted surface of the lower foil,} \\ w(z) &= 0 \text{ as } z \text{ becomes very large.} \end{aligned}\right\} \tag{3}$$

The solution for the complex velocity will be found by means of conformal mapping. The cavitation numbers are then related to the lift coefficients of the plates for various values of the parameters that describe the geometry of the flow.

A Schwarz–Christoffel mapping is employed to transform the problem domain into the upper half of the ζ-plane (figure 3). The mapping is given in differential form as

$$\frac{dz}{d\zeta} = \Gamma(d-c)\,\frac{\zeta(\zeta+1)}{(\zeta-c)(\zeta-d)}, \tag{4}$$

where Γ, c, and d are unknown constants. (4) is integrated to yield

$$z/\Gamma = \zeta(d-c)+d(d+1)\log(\zeta/d-1)-c(c+1)\log(\zeta/c-1). \tag{5}$$

Here, the origins of the z- and ζ-planes are the images of each other, and the point $(-H_2, L)$ in the z-plane corresponds to the point $(-1, 0)$ in the ζ-plane. The

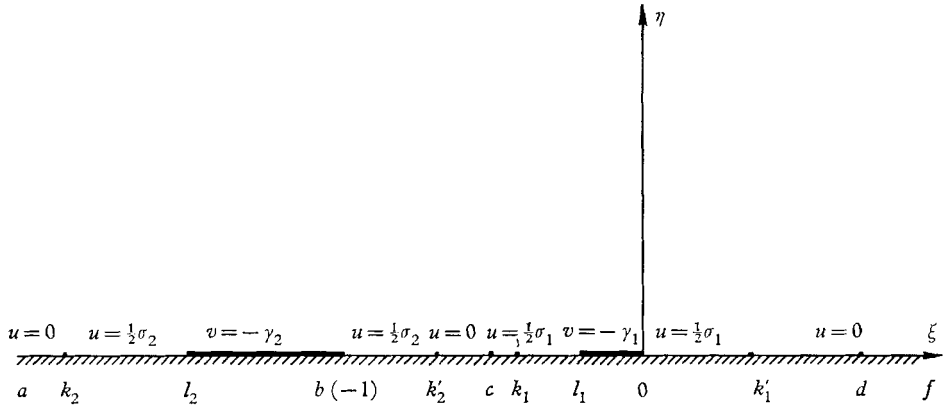

FIGURE 3. The linearized flat-plate problem mapped on to the upper half-plane.

upper cavity end corresponds to the points k_1 and k_1', the lower cavity end to k_2 and k_2', and l_1 and l_2 in the ζ-plane are the images of the plates' trailing edges. The mapping parameters k_1, k_1', k_2, k_2', c, d and Γ are related to H_1, H_2, L_1, L_2 and L in a complicated manner, and these relations must be ascertained numerically. The mechanics of this operation are set forth in appendix 1.

The problem has now been transformed into one of determining a function $w(\zeta)$, analytic in the upper half-plane, which satisfies the following boundary conditions:

$$\left.\begin{aligned}
u(\xi, 0+) &= 0, & -\infty < \xi < k_2,\\
u(\xi, 0+) &= \tfrac{1}{2}\sigma_2, & k_2 < \xi < l_2,\\
v(\xi, 0+) &= -\gamma_2, & l_2 < \xi < -1,\\
u(\xi, 0+) &= \tfrac{1}{2}\sigma_2, & -1 < \xi < k_2',\\
u(\xi, 0+) &= 0, & k_2' < \xi < k_1,\\
u(\xi, 0+) &= \tfrac{1}{2}\sigma_1, & k_1 < \xi < l_1,\\
v(\xi, 0+) &= -\gamma_1, & l_1 < \xi < 0,\\
u(\xi, 0+) &= \tfrac{1}{2}\sigma_1, & 0 < \xi < k_1',\\
u(\xi, 0+) &= 0, & k_1' < \xi < \infty,\\
w(\zeta) &= 0, & \zeta \to \infty.
\end{aligned}\right\} \tag{6}$$

This is a mixed-boundary-value problem, which can be solved by the method discussed by Cheng & Rott (1954). The procedure is to change the problem into one in which the imaginary part of some related analytic function is known at all points on the real axis. A function $H(\zeta)$ is introduced such that, with proper regard for branches,

$$\left.\begin{aligned}
&\operatorname{Re}\{H(\xi,0+)\}=0, && -\infty<\xi<l_2,\\
&\operatorname{Im}\{H(\xi,0+)\}=0, && l_2<\xi<-1,\\
&\operatorname{Re}\{H(\xi,0+)\}=0, && -1<\xi<l_1,\\
&\operatorname{Im}\{H(\xi,0+)\}=0, && l_1<\xi<0,\\
&\operatorname{Re}\{H(\xi,0+)\}=0, && 0<\xi<\infty.
\end{aligned}\right\} \tag{7}$$

A function meeting these requirements is

$$H(\zeta)=i\{\zeta(\zeta-l_1)(\zeta+1)(\zeta-l_2)\}^{\frac{1}{2}}. \tag{8}$$

The boundary conditions for the quotient $w(\zeta)/H(\zeta)$ are

$$\left.\begin{aligned}
&\operatorname{Im}\{w(\zeta)/H(\zeta)\}=0, && -\infty<\xi<k_2,\\
&\operatorname{Im}\{w(\zeta)/H(\zeta)\}=-\tfrac{1}{2}\sigma_2/|H(\xi,0)|, && k_2<\xi<l_2,\\
&\operatorname{Im}\{w(\zeta)/H(\zeta)\}=\gamma_2/|H(\xi,0)|, && l_2<\xi<-1,\\
&\operatorname{Im}\{w(\zeta)/H(\zeta)\}=\tfrac{1}{2}\sigma_2/|H(\xi,0)|, && -1<\xi<k_2',\\
&\operatorname{Im}\{w(\zeta)/H(\zeta)\}=0, && k_2'<\xi<k_1,\\
&\operatorname{Im}\{w(\zeta)/H(\zeta)\}=\tfrac{1}{2}\sigma_1/|H(\xi,0)|, && k_1<\xi<l_1,\\
&\operatorname{Im}\{w(\zeta)/H(\zeta)\}=-\gamma_1/|H(\xi,0)|, && l_1<\xi<0,\\
&\operatorname{Im}\{w(\zeta)/H(\zeta)\}=-\tfrac{1}{2}\sigma_1/|H(\xi,0)|, && 0<\xi<k_1',\\
&\operatorname{Im}\{w(\zeta)/H(\zeta)\}=0, && k_1'<\xi<\infty.
\end{aligned}\right\} \tag{9}$$

In the language of thin-aerofoil theory, this is now a direct thickness problem for the analytic function $w(\zeta)/H(\zeta)$, which may be solved by properly distributing sources on the real axis:

$$w(\zeta)=\frac{H(\zeta)}{\pi}\int_{-\infty}^{+\infty}\frac{\operatorname{Im}\{w(\tau)/|H(\tau)|\}\,d\tau}{\tau-\zeta}, \tag{10}$$

or

$$\frac{\pi w(\zeta)}{H(\zeta)}=\left(-\tfrac{1}{2}\sigma_2\int_{k_2}^{l_2}+\gamma_2\int_{l_2}^{-1}+\tfrac{1}{2}\sigma_2\int_{-1}^{k_2'}+\tfrac{1}{2}\sigma_1\int_{k_1}^{l_1}-\gamma_1\int_{l_1}^{0}-\tfrac{1}{2}\sigma_1\int_{0}^{k_1'}\right)\left(\frac{d\tau}{(\tau-\zeta)\,|H(\tau)|}\right). \tag{11}$$

Any function that is purely real on the ζ-axis may be added to this particular solution. Because of the Kutta condition of smooth trailing-edge separation (Tulin 1953), singularities in $w(\zeta)$ are excluded save at the points corresponding to the leading edges of the foils and the cavity ends. For the linearized double-spiral-vortex model, the jump discontinuities in u at the cavity end necessitate logarithmic singularities in $w(z)$ at these points. These singularities are unaffected by the mapping. A consideration of the velocity vector in the region of the foil leading edges in the physical plane indicates that $z^{-\frac{1}{2}}$ singularities in $w(z)$ are required at the leading edges (Tulin 1964). These singularities are of the type $\zeta^{-\frac{1}{2}}$ in the mapped plane.

The solution—(11)—already includes the desired cavity-end singularities. The correct leading-edge singularities are obtained by adding homogeneous terms of the type $(\zeta-a)^{-1}$ to (11):

$$\frac{\pi w(\zeta)}{H(\zeta)} = \left(-\tfrac{1}{2}\sigma_2\int_{k_2}^{l_2}+\gamma_2\int_{l_2}^{-1}+\tfrac{1}{2}\sigma_2\int_{-1}^{k_2'}+\tfrac{1}{2}\sigma_1\int_{k_1}^{l_1} -\gamma_1\int_{l_1}^{0}-\tfrac{1}{2}\sigma_1\int_{0}^{k_1'}\right)\left(\frac{d\tau}{(\tau-\zeta)\,|H(\tau)|}\right)+\frac{Q_1}{\zeta}+\frac{Q_2}{\zeta+1}. \tag{12}$$

Q_1 and Q_2 are unknown constants that will be part of the full solution. Any other singular terms would change the model and hence are not allowed. Their exclusion can also be defended on the basis of the principle of minimum singularity (Van Dyke 1964). Then too, higher-order leading-edge singularities would result in non-integrable pressure distributions on the foils.

Homogeneous solutions to the transformed problem which are analytic on the x-axis may also be added to (12). Since these solutions must be regular in the upper half-plane, any sum of them can be represented as a single Taylor series $\sum_0^\infty B_n\zeta^n$. Each term of this series can be shown to vanish by a consideration of the behaviour of $w(\zeta)$ at infinity (see below). The solution (12), with two simple poles of unknown strength, is unique (Cheng & Rott 1954).

The perturbation velocity w must equal zero at infinity in the z-plane. The corresponding points in the ζ-plane are at $\zeta = c$, $\zeta = d$, and $\zeta = \infty$. For large ζ, $H(\zeta)$ and the denominators of the separate integrals in (12) are expanded in powers of ζ, and the integrals are treated term by term. The details are presented in appendix 2. The resulting expansion for $w(\zeta)$ is

$$\begin{aligned} i\pi w(\zeta) = {} & \zeta\left\{\left(-\tfrac{1}{2}\sigma_2\int_{k_2}^{l_2}+\gamma_2\int_{l_2}^{-1}+\tfrac{1}{2}\sigma_2\int_{-1}^{k_2'}+\tfrac{1}{2}\sigma_1\int_{k_1}^{l_1}-\gamma_1\int_{l_1}^{0}-\tfrac{1}{2}\sigma_1\int_{0}^{k_1'}\right)\right. \\ & \left.\times\left(\frac{d\tau}{|H(\tau)|}\right)-Q_1-Q_2\right\} \\ & +h_1\left\{\left(-\tfrac{1}{2}\sigma_2\int_{k_2}^{l_2}+\gamma_2\int_{l_2}^{-1}+\tfrac{1}{2}\sigma_2\int_{-1}^{k_2'}+\tfrac{1}{2}\sigma_1\int_{k_1}^{l_1}-\gamma_1\int_{l_1}^{0}-\tfrac{1}{2}\sigma_1\int_{0}^{k_1'}\right)\left(\frac{d\tau}{|H(\tau)|}\right)-Q_1-Q_2\right\} \\ & +\left(-\tfrac{1}{2}\sigma_2\int_{k_2}^{l_2}+\gamma_2\int_{l_2}^{-1}+\tfrac{1}{2}\sigma_2\int_{-1}^{k_2'}+\tfrac{1}{2}\sigma_1\int_{k_1}^{l_1}-\gamma_1\int_{l_1}^{0}-\tfrac{1}{2}\sigma_1\int_{0}^{k_1'}\right)\left(\frac{\tau\,d\tau}{|H(\tau)|}\right)+Q_2+\ldots, \end{aligned} \tag{13}$$

where $-iH(\zeta) = \zeta^2+h_1\zeta+\ldots$.

Setting the ζ and constant terms of this expansion equal to zero yields the equations

$$\left(-\tfrac{1}{2}\sigma_2\int_{k_2}^{l_2}+\gamma_2\int_{l_2}^{-1}+\tfrac{1}{2}\sigma_2\int_{-1}^{k_2'}+\tfrac{1}{2}\sigma_1\int_{k_1}^{l_1}-\gamma_1\int_{l_1}^{0}-\tfrac{1}{2}\sigma_1\int_{0}^{k_1'}\right)\left(\frac{d\tau}{|H(\tau)|}\right)-Q_1-Q_2 = 0, \tag{14}$$

and

$$\left(-\tfrac{1}{2}\sigma_2\int_{k_2}^{l_2}+\gamma_2\int_{l_2}^{-1}+\tfrac{1}{2}\sigma_2\int_{-1}^{k_2'}+\tfrac{1}{2}\sigma_1\int_{k_1}^{l_1}-\gamma_1\int_{l_1}^{0}-\tfrac{1}{2}\sigma_1\int_{0}^{k_1'}\right)\left(\frac{\tau\,d\tau}{|H(\tau)|}\right)+Q_2 = 0. \tag{15}$$

Equations (14) and (15) guarantee that $w(\zeta)$ behaves as $1/\zeta$ for large ζ. At $\zeta = c$, the condition that $w(\zeta)$ vanish is expressed as

$$\left(-\tfrac{1}{2}\sigma_2\int_{k_2}^{l_2}+\gamma_2\int_{l_2}^{-1}+\tfrac{1}{2}\sigma_2\int_{-1}^{k_2'}+\tfrac{1}{2}\sigma_1\int_{k_1}^{l_1}-\gamma_1\int_{l_1}^{0}-\tfrac{1}{2}\sigma_1\int_{0}^{k_1'}\right) \times\left(\frac{d\tau}{(\tau-c)\,|H(\tau)|}\right)+\frac{Q_1}{c}+\frac{Q_2}{1+c}=0. \tag{16}$$

Similarly, at $\zeta = d$,

$$\left(-\tfrac{1}{2}\sigma_2\int_{k_2}^{l_2}+\gamma_2\int_{l_2}^{-1}+\tfrac{1}{2}\sigma_2\int_{-1}^{k_2'}+\tfrac{1}{2}\sigma_1\int_{k_1}^{l_1}-\gamma_1\int_{l_1}^{0}-\tfrac{1}{2}\sigma_1\int_{0}^{k_1'}\right) \times\left(\frac{d\tau}{(\tau-d)\,|H(\tau)|}\right)+\frac{Q_1}{d}+\frac{Q_2}{1+d}=0. \tag{17}$$

(14)–(17) are solved numerically for the unknowns σ_1, σ_2, Q_1 and Q_2. It is convenient that all the coefficients in these four equations are expressible in terms of elliptic integrals, as illustrated in appendix 3. The inverse nature of this method should be noted, as it results in a large increase in computer time when certain calculations are performed. This is particularly true when both cavitation numbers are kept constant and the depth of one or both foils is varied. The basic results provided herein serve to aid the user in his selection of variables and thus to reduce the computation effort required for further work.

The non-dimensional lift and drag coefficients are, respectively,

$$C_{Li} = L_i/\tfrac{1}{2}\rho U^2,$$

and

$$C_{Di} = D_i/\tfrac{1}{2}\rho U^2,$$

where L_i and D_i are the lift and drag on body i. To the order of approximation implied in the linearization, L_i equals the normal pressure force on the body and D_i is that force multiplied by the angle of attack. Thus, for a flat-plate hydrofoil,

$$D_i = \gamma_i L_i.$$

The normal force N_i is given by the pressure integral over the body

$$N_i = \int_i \{p(x, y_b-) - p(x, y_b+)\}\,dx.$$

The lift coefficients are then

$$C_{L1} = \int_0^1 \{p(x, 0-) - p(x, 0+)\}\,dx/(\tfrac{1}{2}\rho U^2),$$

and

$$C_{L2} = \int_{L-iH_2}^{L+1-iH_2} \{p(x, -H_2-) - p(x, -H_2+)\}\,dx/(\tfrac{1}{2}\rho U^2).$$

Using the definition of the cavitation number, these expressions can be shown to be equivalent to

$$C_{L1} = \sigma_1 - 2\int_0^1 u(x, 0-)\,dx, \tag{18a}$$

and

$$C_{L2} = \sigma_2 - 2\int_{L-iH_2}^{L+1-iH_2} u(x, -H_2-)\,dx. \tag{18b}$$

From the mapping

$$dx = \frac{\Gamma(d-c)\,\zeta(\zeta+1)}{(\zeta-c)\,(\zeta-d)}\,d\zeta,$$

$$C_{L1} = \sigma_1 + \frac{2\Gamma(d-c)}{\pi}\left\{\int_0^{l_1} G(\xi)\left(-\tfrac{1}{2}\sigma_2\int_{k_2}^{l_2} + \gamma_2\int_{l_2}^{-1} + \tfrac{1}{2}\sigma_2\int_{-1}^{k_2'} + \tfrac{1}{2}\sigma_1\int_{k_1}^{l_1}\right.\right.$$
$$\left.-\gamma_1\int_{l_1}^{0} - \tfrac{1}{2}\sigma_1\int_0^{k_1'}\right)\left(\frac{d\tau}{(\tau-\xi)\,|H(\tau)|}\right)d\xi + Q_1\int_0^{l_1}\frac{(\xi+1)\,|H(\xi)|\,d\xi}{(\xi-c)\,(\xi-d)}$$
$$\left.+\,Q_2\int_0^{l_1}\frac{\xi\,|H(t)|\,d\xi}{(\xi-c)\,(\xi-d)}\right\}, \tag{19}$$

and $$C_{L2} = \sigma_2 - \frac{2\Gamma(d-c)}{\pi}\left\{\int_{-1}^{l_2} G(\xi)\left(-\tfrac{1}{2}\sigma_2\int_{k_2}^{l_2} + \gamma_2\int_{l_2}^{-1} + \tfrac{1}{2}\sigma_2\int_{-1}^{k_2'} + \tfrac{1}{2}\sigma_1\int_{k_1}^{l_1}\right.\right.$$
$$\left.-\gamma_1\int_{l_1}^{0} - \tfrac{1}{2}\sigma_1\int_0^{k_1'}\right)\left(\frac{d\tau}{(\tau-\xi)\,|H(\xi)|}\right)d\xi + Q_1\int_{-1}^{l_2}\frac{(\xi+1)\,|H(\xi)|\,d\xi}{(\xi-c)\,(\xi-d)}$$
$$\left.+\,Q_2\int_{-1}^{l_2}\frac{\xi\,|H(\xi)|\,d\xi}{(\xi-c)\,(\xi-d)}\right\}, \tag{20}$$

where $$G(\xi) = \frac{\xi(\xi+1)\,|H(\xi)|}{(\xi-c)\,(\xi-d)}.$$

With some obvious substitutions, these expressions become

$$C_{L1} = \sigma_1 - \frac{2\Gamma(d-c)}{\pi}$$
$$\times\,(\tfrac{1}{2}\sigma_2 K1 - \gamma_2 K2 - \tfrac{1}{2}\sigma_2 K3 - \tfrac{1}{2}\sigma_1 K4 + \gamma_1 K5 + \tfrac{1}{2}\sigma_1 K6 - Q_1 K7 - Q_2 K8), \tag{21}$$

and

$$C_{L2} = \sigma_2 + \frac{2\Gamma(d-c)}{\pi}$$
$$\times\,(\tfrac{1}{2}\sigma_2 J1 - \gamma_2 J2 - \tfrac{1}{2}\sigma_2 J3 - \tfrac{1}{2}\sigma_1 J4 + \gamma_1 J5 + \tfrac{1}{2}\sigma_1 J6 - Q_1 J7 - Q_2 J8). \tag{22}$$

The inner integrals of $K5$ and $J2$ must be treated as Cauchy principal-value integrals. As with the equations that determine the cavitation-number cavity-length relationships, it is convenient for the numerical work that the inner integrals in (21) and (22) can be expressed in terms of elliptic integrals. The calculation of C_{L1} and C_{L2} is discussed further in appendix 4.

It should be noted that body shapes other than flat plates can be handled with little additional effort. For example, any shape that can be expressed as a rational function of the physical horizontal-distance variable x will allow a similar treatment, as the coefficients of σ_1, σ_2, Q_1 and Q_2 in (14), (15), (16), and (17), and the inner integrals in (21) and (22), can still be expressed in terms of elliptic integrals. Also, no further singularities (see appendix 4) are introduced in any of the integrands in (21) and (22).

3. Results and conclusions

In view of the wealth of variable physical parameters γ_1, γ_2, H_1, H_2, L, σ_1, σ_2, a wide variety of situations can be studied. It seems reasonable to confine attention to three quite different practical configurations that illustrate the more

important physical effects. The effects that are expected to parallel those investigated by Yim (1964) will not be considered. Thus, the angles of attack are held constant, and the total system of the two hydrofoils is not moved vertically in relation to the free surface. In this spirit, the representative cases shown in figure 4 will be investigated.

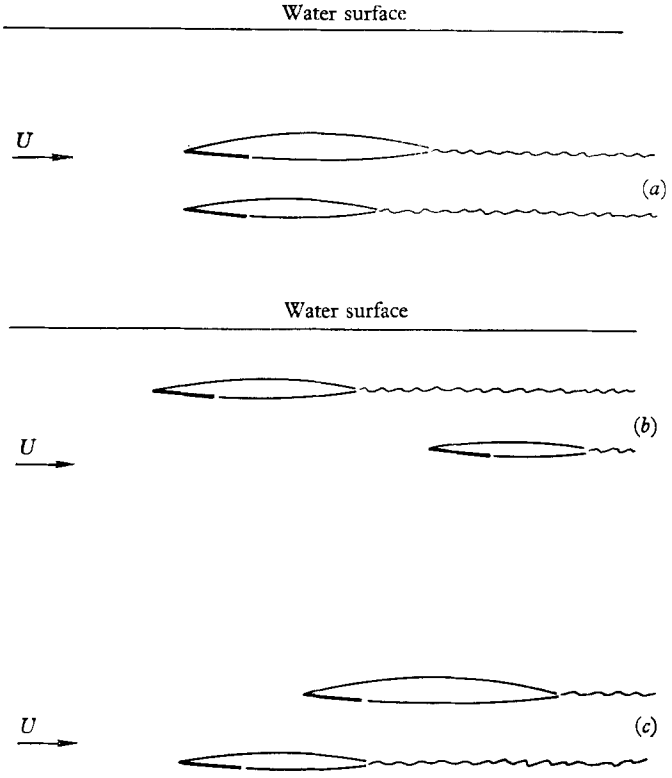

FIGURE 4. Two-foil representative cases. (*a*) Case I, shallow stacked foils; (*b*) case II, shallow staggered foils, shown with positive stagger; (*c*) case III, deeply submerged staggered foils, shown with negative stagger.

Case I. Shallow stacked foils

The two foils are aligned vertically and are rather close to the free water surface. On a hydrofoil vessel, this would correspond to having the two foils supported by the same strut system. The fixed physical parameters are $\gamma_1 = \gamma_2 = 5°$, $H_1 = 2{\cdot}0$, $H_2 = 1{\cdot}0$, $L = 0$. The effect of cavitation-number variation on lift coefficients and cavity lengths is studied.

Figure 5 shows the effect on the two cavity lengths of changing the upper cavitation number. The lower cavitation number is held constant. Figure 6 is the counterpart of figure 5 when the lower cavitation number is varied. In figure 7, the cavity lengths are shown as functions of equal, changing cavitation numbers. In each plot, the dotted lines depict the result calculated by ignoring the other foil and using the single-foil theory due to Yim (1964).

In general, the lower-cavity length is decreased by the presence of the upper foil. Mathematically, this result stems from the vertical-perturbation-velocity

boundary condition on the lower side of the upper foil. Physically, the downwash from the upper foil tends to decrease the effective angle of attack of the lower foil and hence decreases the cavity length. (In the linearized theory of supercavitating hydrofoils, the cavity length is linearly proportional to the angle of attack.)

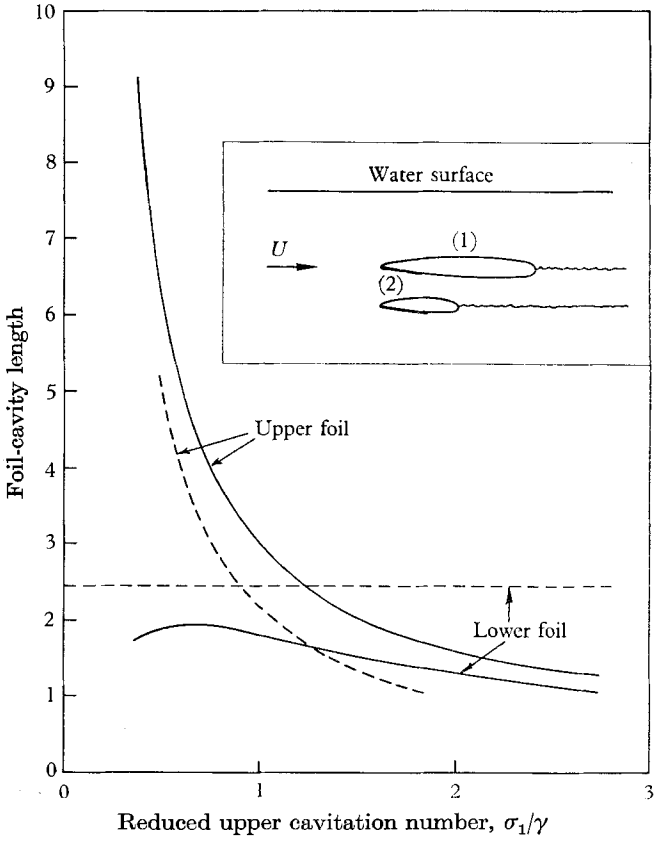

FIGURE 5. Shallow-stacked-foil case: foil-cavity lengths against reduced upper cavitation number, for constant lower cavitation number $\sigma_2 = 0{\cdot}082$. The inset, showing the configuration, is drawn to scale. ——, present analysis; – – –, Yim (1964).

On the other hand, the upper cavity length is always increased as a result of interaction effects. Now the positive vertical perturbation velocity associated with the front part of the lower cavity increases the effective angle of attack of the upper foil.

In figures 5 and 6, the lengths of the cavities in which the pressure is held constant are seen to increase or decrease with an increase of the other, variable, cavitation number, depending upon the magnitude of that cavitation number. This result probably stems from the mutual approach and subsequent recession of the two turbulent mixing regions associated with the ends of the cavities.

Figures 8–10 show the separate and total lift coefficients of the system in the same three situations as above. Again, the dotted lines represent results calculated after Yim (1964). In general, the lift on the upper foil is decreased because of the nearness of the low-pressure region around the lower cavity; the lift on the

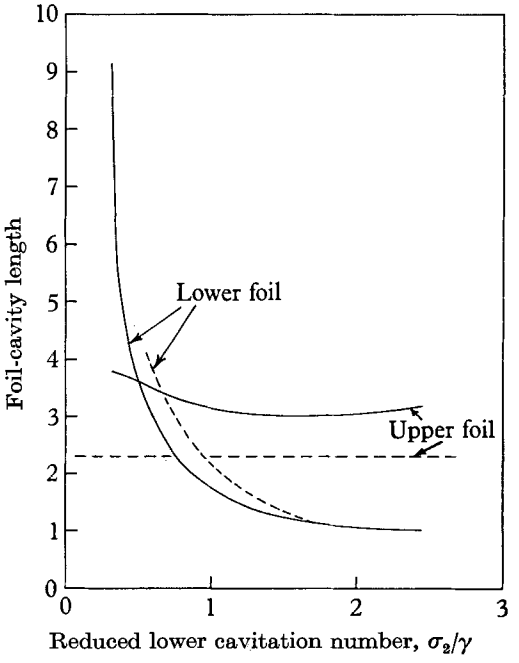

FIGURE 6. Shallow-stacked-foil case: foil-cavity lengths against reduced lower cavitation number, for constant upper cavitation number $\sigma_1 = 0{\cdot}082$. ——, present analysis; – – –, Yim (1964).

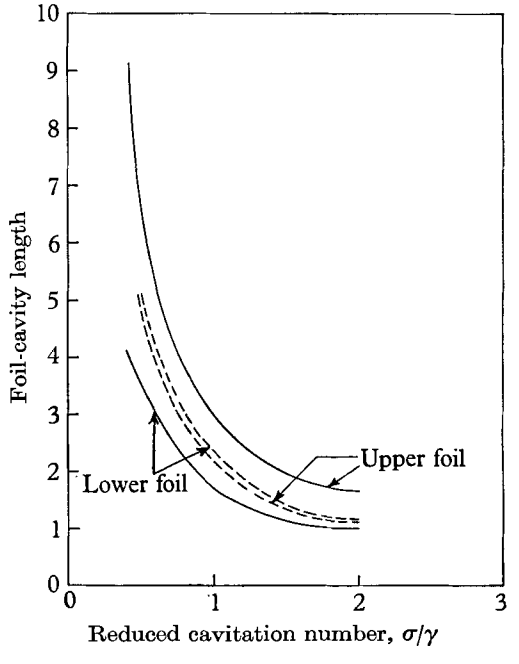

FIGURE 7. Shallow-stacked-foil case: foil-cavity lengths against reduced cavitation number, for equal cavitation numbers. ——, present analysis; – – –, Yim (1964).

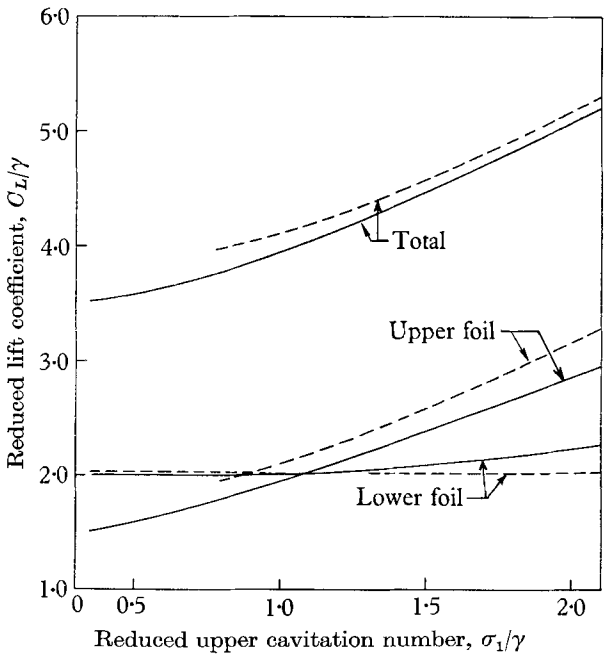

FIGURE 8. Shallow-stacked-foil case: reduced lift coefficients against reduced upper cavitation number, for constant lower cavitation number $\sigma_2 = 0{\cdot}082$. ——, present analysis; – – –, Yim (1964) with uncoupled foils.

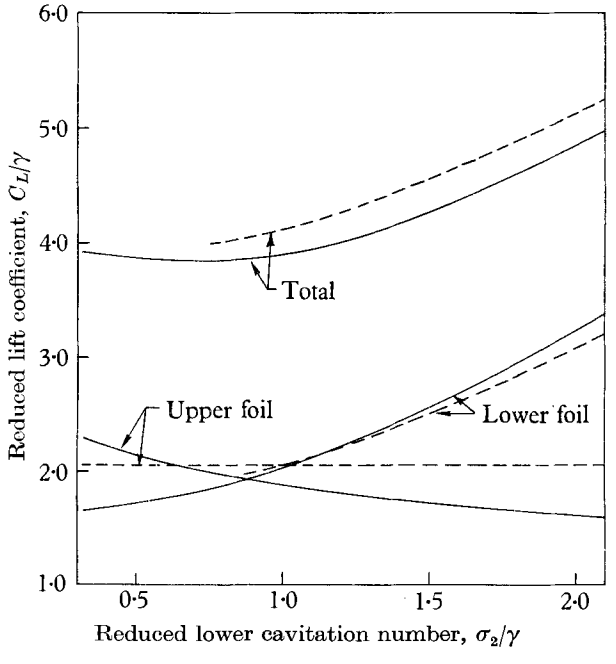

FIGURE 9. Shallow-stacked-foil case: reduced lift coefficients against reduced lower cavitation number, for constant upper cavitation number $\sigma_1 = 0{\cdot}082$. ——, present analysis; – – –, Yim (1964) with uncoupled foils.

lower foil is seen to increase because of the increase in pressure resulting from the general decrease in flow velocity brought about by the addition of a second stagnation point in the flow on the upstream foil. This effect overcomes the effect of the downwash from the upper foil, which decreases the effective angle of attack of the lower foil and hence tends to decrease the lift.

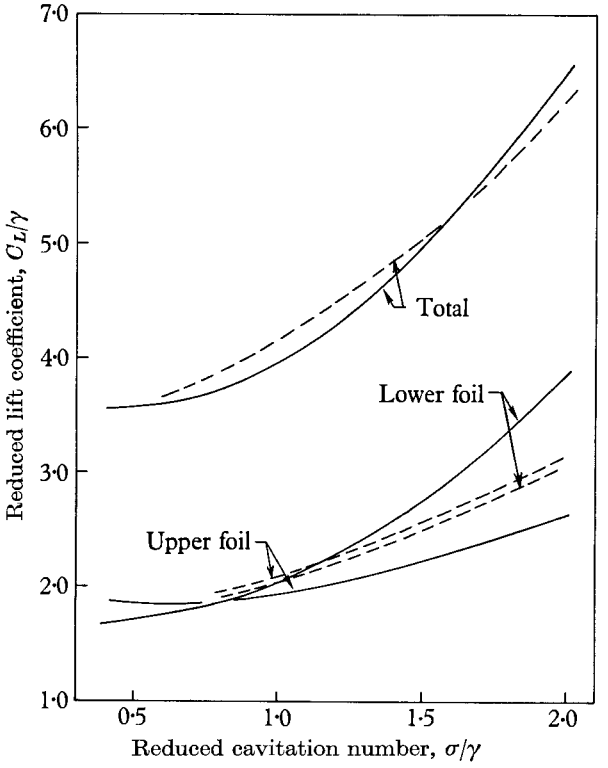

FIGURE 10. Shallow-stacked-foil case: reduced lift coefficients against reduced cavitation number, for equal cavitation numbers. ——, present analysis; – – –, Yim (1964) with uncoupled foils.

The opposite interaction effects on the separate foils usually produce a slight decrease in total system lift, but obviously the total system moments are changed more noticeably. Hsieh (1964), in an analysis of a similar situation involving infinite cavities, finds the same behaviour of the lift coefficients in a comparable situation where, in the present nomenclature, $L = 0$, $H_1 = 1{\cdot}0$, and $H_2 = 0{\cdot}5$.

For completeness, the foil leading-edge-singularity strengths have been plotted for the situation in which both cavitation numbers were varied (figure 11). Here, the dotted line shows the leading-edge singularity strength of a single, flat-plate, supercavitating hydrofoil in an infinite fluid. The free-surface and foil-interaction effects result in an increase of the singularity strengths.

Case II. Shallow staggered foils

The two foils are closer to the water surface than in case I and are quite far apart horizontally. This arrangement simulates a typical hydrofoil-boat configuration

in which the foils are supported by independent fore-and-aft strut systems. Here, the fixed physical parameters are $\gamma_1 = \gamma_2 = 5°$, $H_1 = 1{\cdot}0$, $L = 4{\cdot}5$. Again, the effect of cavitation-number variation is considered. Also, the depth of the downstream foil is varied, and the corresponding lift coefficients and cavity lengths are calculated for fixed cavitation numbers.

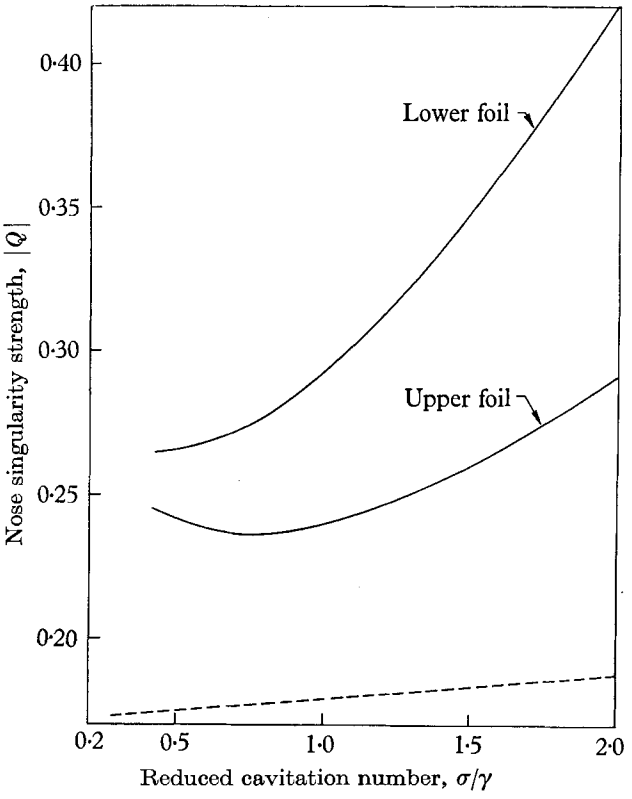

FIGURE 11. Shallow-stacked-foil case: nose-singularity strengths against reduced cavitation number, for equal cavitation numbers. ——, present analysis; – – –, result for one flat plate in an infinite fluid.

In this configuration the downstream foil is operating near the wake generated by the upstream foil, and not near the upstream foil itself. In the linearized double-spiral-vortex model, the boundary condition enforced in the wakes is the same as that on the water surface. Thus, the behaviour of the downstream foil is expected to approximate that of a single foil near a free surface.

Figures 12 and 13 show the effect on cavity lengths of varying one cavitation number while holding the other cavitation number constant. Here again, the lower, downstream cavity is shortened and the upper, upstream cavity is lengthened in comparison with single-body results after Yim (1964). The physical explanation for the lengthening of the upstream cavity follows that offered in case I. As for the shortening of the lower cavity, the decrease in effective angle of attack of the lower foil is now due to the warping of the upstream cavity and wake in conjunction with the lift exerted on the upper foil (Tulin 1964). Both

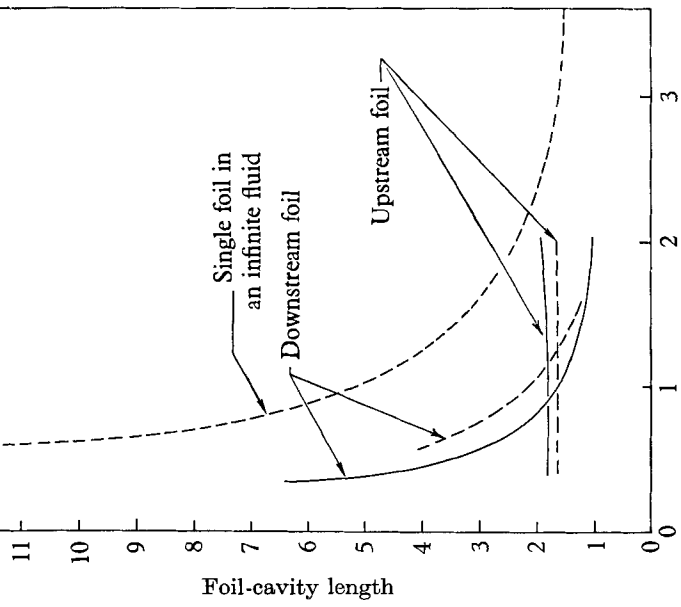

FIGURE 13. Shallow-staggered-foil case: foil-cavity lengths against reduced downstream cavitation number, for constant upstream cavitation number $\sigma_1 = 0{\cdot}1$. ——, present analysis; – – –, Yim (1964).

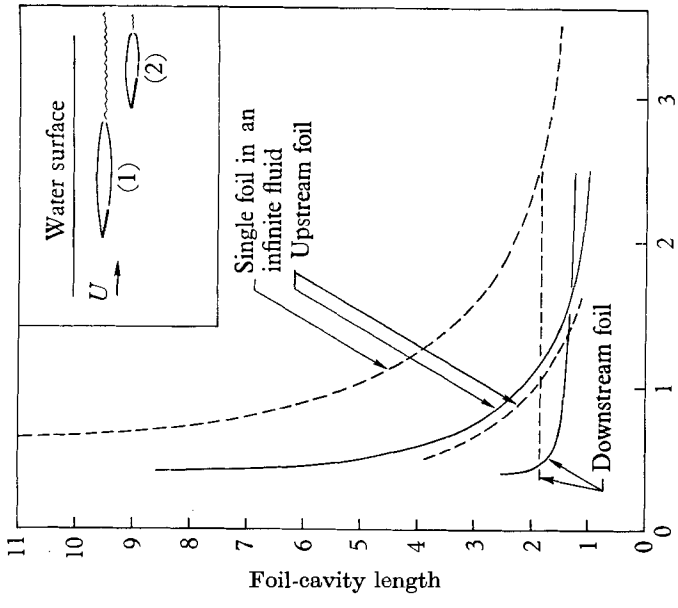

FIGURE 12. Shallow-staggered-foil case: foil-cavity lengths against reduced upstream cavitation number, for constant downstream cavitation number $\sigma_2 = 0{\cdot}1$. The inset, showing the configuration, is drawn to scale. ——, present analysis; – – –, Yim (1964).

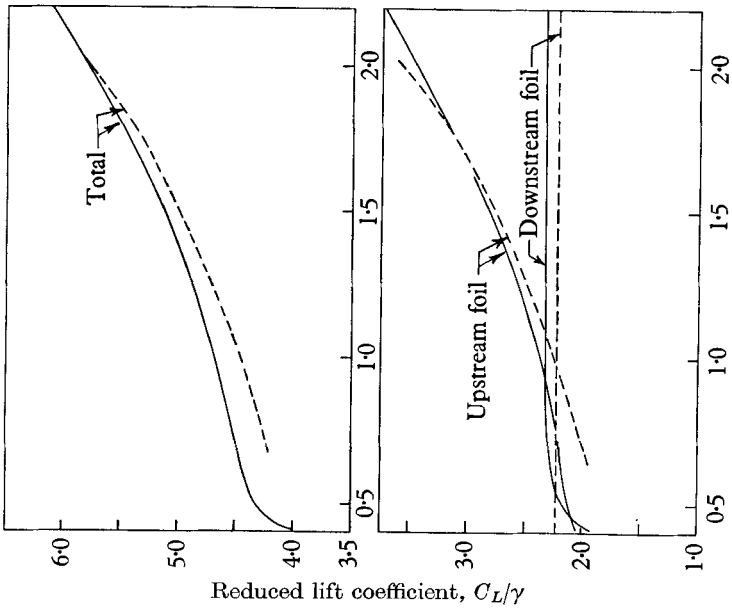

FIGURE 15. Shallow-staggered-foil case: reduced lift coefficient against reduced upstream cavitation number, for constant downstream cavitation number $\sigma_2 = 0{\cdot}1$. ——, present analysis; – – –, Yim (1964) with uncoupled foils.

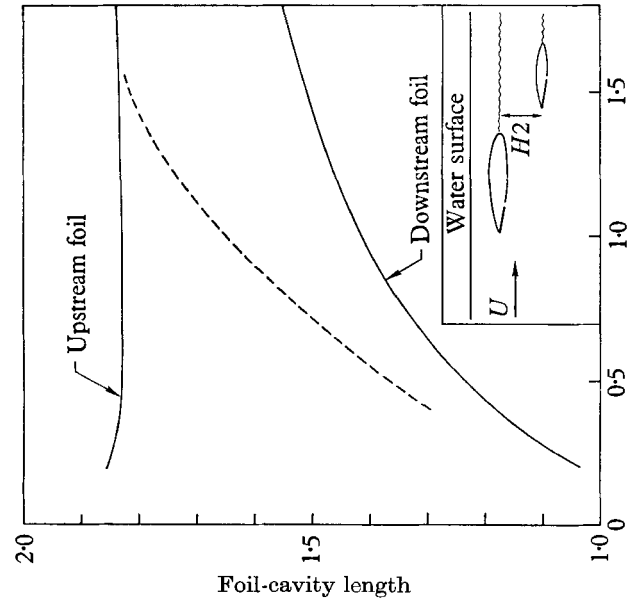

FIGURE 14. Shallow-staggered-foil case: foil-cavity lengths against depth of downstream foil, for equal cavitation numbers $\sigma = 0{\cdot}1$. The inset is drawn to scale. ——, present analysis; – – –, equivalent free surface results after Yim (1964).

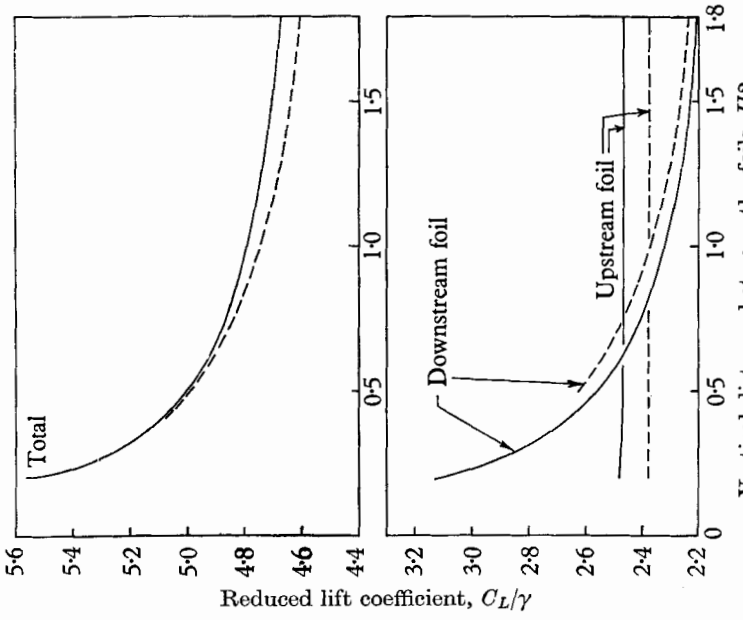

FIGURE 17. Shallow-staggered-foil case: reduced lift coefficients against downstream foil depth, for constant cavitation numbers $\sigma = 0{\cdot}1$. ——, present analysis; – – –, uncoupled foil and equivalent-free-surface results after Yim (1964).

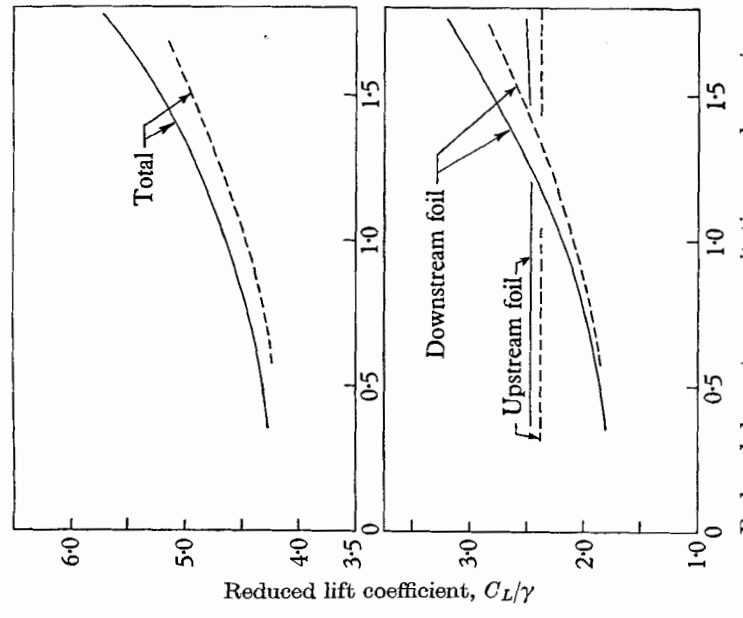

FIGURE 16. Shallow-staggered-foil case: reduced lift coefficient against reduced downstream cavitation number, for constant upstream cavitation number $\sigma_1 = 0{\cdot}1$. ——, present analysis; – – –, Yim (1964) with uncoupled foils.

cavities are significantly shorter than the plotted result for a single flat-plate hydrofoil in an infinite fluid. The length of the upstream cavity is essentially independent of changes in the downstream cavitation number, as expected, while the downstream-cavity length increases markedly when the turbulent flow associated with the end of the upstream cavity passes the leading edge of the downstream foil. Here the upstream cavity is accompanied by a pressure reduction in the surrounding fluid. The normal tendency of the fluid pressure to close the cavity is then decreased.

Figure 14 shows the effect on both cavity lengths when the cavitation numbers are kept constant and the depth of the downstream foil is varied. Little effect was found on the length of the upstream cavity. The downstream cavity experiences a considerable shortening as the vertical distance between the foils approaches zero. A consideration of Yim's work shows that this shortening is to be expected on the basis of the equivalence of the boundary conditions applied in wakes and on free surfaces. The dotted line indicates the result obtained by replacing the upper-body-cavity wake by an 'equivalent free surface' at the same depth, and then using single-body results based on Yim.

Unfortunately, in this case II (where the upstream foil is a unit distance from the free water surface), accuracy considerations related to the sensitivity of the mapping prevented computations for situations in which the downstream foil was the upper foil (appendix 1). Otherwise, it is not crucial, in general, whether L is positive or negative (see case III below) as far as the computations are concerned.

Figures 15 and 16 show that the lifts on the separate foils are always increased here, unlike the case involving stacked foils. Hsieh (1964) reports no equivalent results with which to compare these findings, although they can easily be explained by the fact that the wake acts as a free surface. Figure 16 indicates that changing the downstream cavitation number has the expected negligible effect on the upstream lift coefficient. Figure 15 shows a substantial change in the behaviour of both lift coefficients as the end of the upstream cavity nears and passes the downstream foil. The downstream lift is reduced dramatically as a result of the low pressure associated with the upstream cavity, while the decrease of the upstream lift stemming from the decrease of the corresponding cavitation number is allayed.

Figure 17 indicates that the upstream lift is virtually unchanged by a vertical displacement of the downstream foil. The downstream lift rises markedly as that foil approaches the wake generated by the upstream foil. Again, the 'equivalent-free-surface' result is plotted, and shows that in this case calculations of the downstream lift can be performed to an accuracy of 5% by the use of such an artifice.

Case III. Deeply submerged staggered foils

The foils are taken far from the free water surface in order to isolate the effect of their mutual proximity. The (normalized) depth of the upstream foil is 100. The other fixed physical parameters are $\gamma_1 = \gamma_2 = 5°$, $|L| = 2{\cdot}0$, $\sigma_1 = \sigma_2 = 0{\cdot}1$. The downstream-foil depth relative to the fixed upstream foil is varied, and the lift coefficients and cavity lengths are calculated.

Here the flow regime is quite unlike that in the previous example, because of the absence of the free surface and the greater lengths of the cavities. In particular, the end of the upstream cavity now lies downstream of the trailing foil. In figure 18, both cavities are seen to undergo a sharp increase in length as the trailing foil passes downward through the upstream cavity. Again, the down-

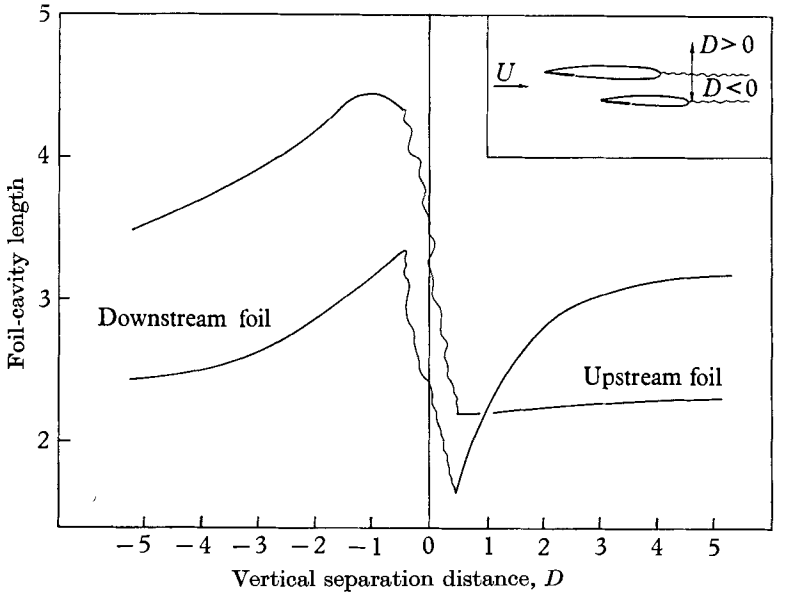

FIGURE 18. Deep-submergence case: foil-cavity lengths against vertical distance between the foils, for constant cavitation numbers $\sigma = 0{\cdot}1$. The inset is drawn to scale.

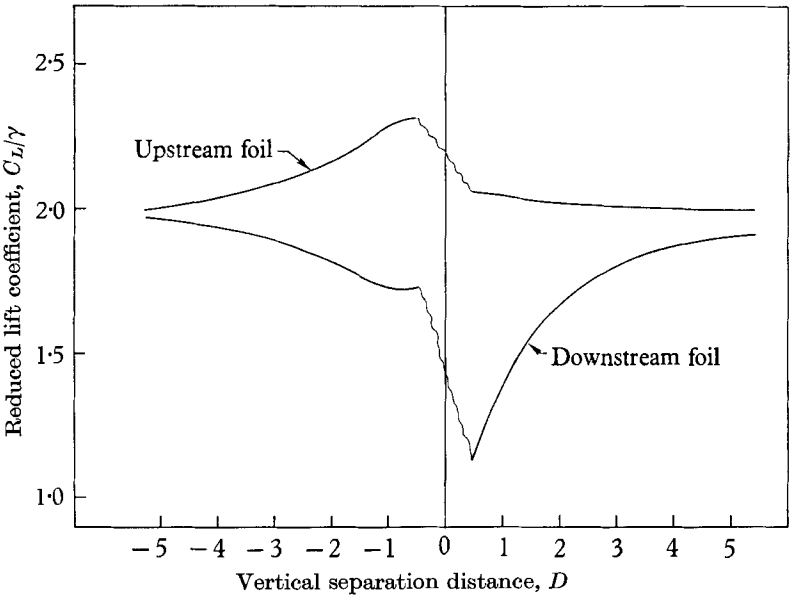

FIGURE 19. Deep-submergence case: reduced lift coefficients against vertical distance between the foils, for constant cavitation numbers $\sigma = 0{\cdot}1$.

wash from the leading upper foil results in a shortening of the trailing lower cavity. Now the downstream-cavity length either increases or decreases as the upstream system is approached vertically, according to whether the trailing foil is below or above the leading foil. There is little effect on the lower upstream cavity as a result of a relative change in vertical position. Fairly large cavity interactions are predicted even when large distances separate the two foils.

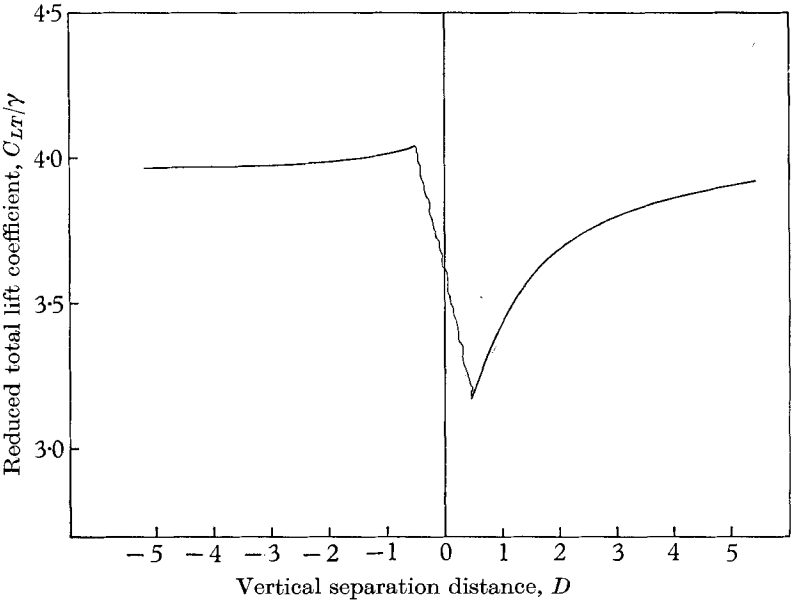

FIGURE 20. Deep-submergence case: total reduced lift coefficient against vertical distance between the foils, for constant cavitation numbers $\sigma = 0{\cdot}1$.

In figure 19, the individual lift coefficients also show a strong discontinuity across the upstream cavity. An abrupt increase in both lifts is forecast as the trailing foil moves in a downward direction through the upstream cavity. The downstream lift coefficient shows the larger jump, because of the high speeds and low pressures associated with the upstream cavity. This low pressure is felt on the downstream, upper foil, but is masked by the downstream cavity when the downstream foil is the lower of the two foils. Of course, the discontinuity is also present in the total lift of the system, as shown in figure 20. However, as with the stacked foils, the changes (because of interaction effects in the individual lifts) tend to compensate each other.

4. General conclusions

The trends examined are not expected to resemble closely those reported by Hsieh (1964), as the cavities in the present work are areas in which the lowest pressure in the flow is achieved (Birkhoff & Zarantonello 1957), whereas, when infinite cavities are used, the pressure in the cavities equals the pressure on the free surface.

When the upstream cavity does not pass the downstream foil, the characteristic features of the upstream foil are unaffected by changes in the vertical height and cavitation number of the downstream foil. In general, the interaction effects on cavity lengths and lift coefficients are quite dependent on the length of the upstream cavity.

The downwash from the upper, leading foil always tends to shorten the lower, trailing cavity. On the other hand, the lower trailing foil produces a longer upstream cavity. These effects are usually also present when the upstream foil is the lower foil.

When the horizontal distance between the two foils is small, the interaction effects on the separate lifts tend to cancel each other so that the total lift calculated by using the uncoupled theory is usually accurate to within 6 %. Whether or not this accuracy is acceptable depends on the particular application.

There is a large discontinuity in individual and total lifts and in cavity lengths of the system connected with a motion of the trailing foil through the cavity of the leading foil. When fairly low cavitation numbers are involved, the downstream foil should be the lower of the two for larger values of the total lift.

With the shallow stacked foils, there is a larger change in total lift when the upper-cavity pressure is varied than when the lower-cavity pressure is varied. Therefore it is more advantageous to control the upper cavitation number than the lower to produce desired changes in lift.

In each situation studied, the interaction effects on the individual-foil moments (taken to be positive in a counterclockwise direction) are qualitatively the same as the effects on the foil lifts. The actual moment calculations could be performed by applying the separate lift forces at the centres of pressure of the two foils (Parkin 1959). These centres are approximately at the foil quarter-chord points (Parkin 1959). The total moment taken about the leading edge of the upstream foil will be increased when the horizontal distance separating the two foils is large (case II) and decreased when this distance is small (case I).

Again, a sharp change in total moment is predicted when the the trailing foil moves vertically through the leading-foil wake. Thus it is expected that a downward, plunging motion of the bow of a hydrofoil vessel, which results in a reversal in the relative vertical positions of the two foils, will be retarded by a concurrent decrease in the counterclockwise moment on the system. Figure 21 illustrates a plunging vessel. Note that this situation does not exactly duplicate that studied using the theory, as now the angles of attack also change. Also, the total moment will increase when the motion of the vessel leads to the trailing foil passing downward through the upstream cavity. Hence, there is a stabilizing effect on each type of motion. Naturally, these conclusions are invalid if the motion results in either of the cavities being re-formed on the lower surface of the foil.

It is reasonable to ask how the use of a different linearized model would affect the results discussed above. Several non-linear models are shown in figure 22, and their linearized counterparts are presented in figure 23. In the first place, some alternative models would present purely mathematical difficulties. For instance, the absence of a wake on which conditions are specified in the Tulin

closed-cavity model (figure 23) precludes the direct application of the method of Cheng & Rott (1954). Secondly, the linearized double-spiral-vortex model that has been employed in the analysis has a number of pleasing features. There is

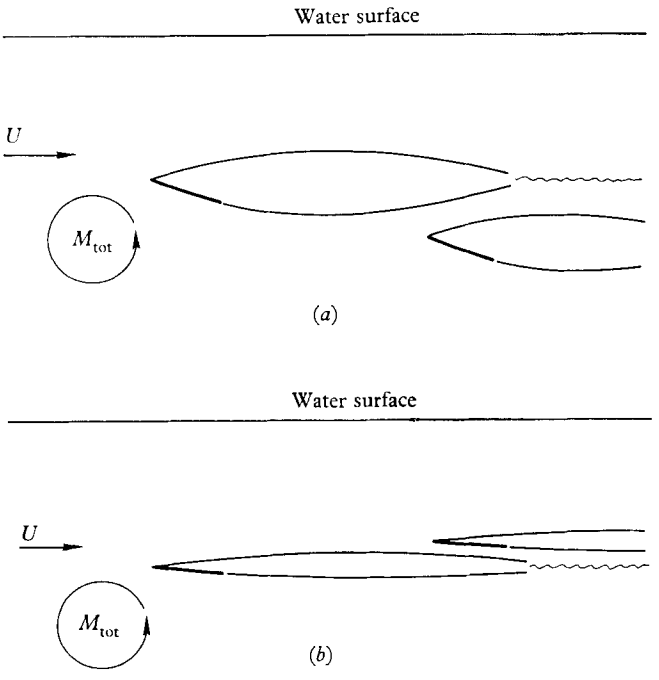

FIGURE 21. Stability of a plunging hydrofoil boat. (*a*) Foil geometry before bow plunge; (*b*) foil geometry after bow plunge. $M_a > M_b$, giving a net restoring moment.

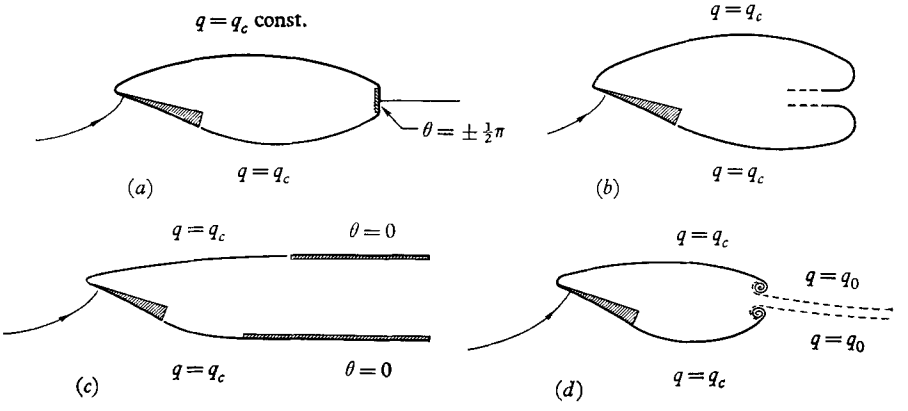

FIGURE 22. Models of finite-length cavity flows. (*a*) Modified Riabouchinsky model; (*b*) re-entrant-jet model; (*c*) horizontal-plate-termination model (Roshko model); (*d*) double-spiral-vortex model.

a trailing wake: its width decreases to zero at infinity, and the loss in pressure as a result of the turbulent conditions at the cavity end is reproduced. Tulin (1964) has given a complete discussion of this model. On the other hand, the linearized Roshko model shown in figure 23—which could also be treated by the method of

Cheng & Rott—has a 'wake' that seems too wide when compared with experiments, and does not allow the downward warping of the wake which is known to accompany lifting forces on the foil. The linearized double-spiral-vortex model stands out as the best attempt to date to represent adequately the flow conditions near the limiting boundaries.

Nevertheless, it remains worth while to discuss the effect of the use of different models on lift and cavity results. Of course, a closed-cavity model that does not allow a wake will not feature the distinctive stabilizing phenomenon involved in plunging (see above). Note that both the re-entrant jet model and the modified Riabouchinsky model (figure 22) degenerate to the Tulin closed-cavity model

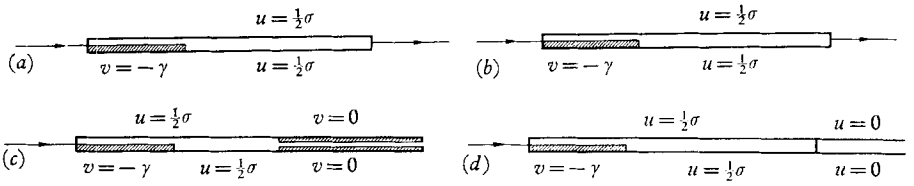

FIGURE 23. Linearized models of finite-length cavity flows. $\sigma = \{\pi - p(\text{cavity})\}/\frac{1}{2}\rho U^2$. (*a*) Linearized modified Riabouchinsky model (Tulin closed-cavity model); (*b*) linearized re-entrant-jet model; (*c*) linearized horizontal-plate-termination model (linearized Roshko model); (*d*) linearized double-spiral-vortex model.

after linearization. Also, use of either the Tulin closed-cavity model or the linearized Roshko model would lead to smaller foil lifts. In these alternative models, u decreases monotonically from $\frac{1}{2}\sigma$ on the cavity walls to zero at infinity, whereas u is taken to be zero throughout the wake in the linearized double-spiral-vortex model. Since u is a harmonic function, these higher wake-region values in the two alternative models would result in an increase of u on the wetted surface of the foil, and hence lower the pressure on the wetted surface.

Yim has reported that the linearized double-spiral-vortex model leads to cavity lengths that are in excellent agreement with the experimental results of Dawson & Bate (1962). The Tulin model seems consistently to underestimate the cavity length, and the Roshko model has no well-defined cavity length. Yim's theory shows fairly good agreement with experimental lift coefficients as well. The only experimental work dealing with two cavitating bodies near a free surface known to the authors is Wetzel (1965). Unfortunately, it does not invite comparison with the present theory because the tested foils had an aspect ratio of only 2 (highly three-dimensional flow) and at that the only possibly comparable case has negligible interaction effects.

This research was carried out at Stanford University under the Bureau of Ships General Hydromechanics Research Program, and National Science Foundation Grant No. NSF-GP 948 provided support for the numerical computations. Reproduction in whole or in part is permitted for any purpose of the United States Government.

Appendix 1. The Schwarz–Christoffel mapping

The correspondence between the z- and ζ-planes is given by the function

$$z/\Gamma = \zeta(d-c)+d(d+1)\log(\zeta/d-1)-c(c+1)\log(\zeta/c-1). \tag{A 1.1}$$

Here the points at infinity and the origins have been made to coincide, and the z-point $(L, -H_2)$ is mapped into the ζ-point $(-1, 0)$ (see figures 2, 3).

Derived from (A 1.1), the equations that determine the parameters c, d, and Γ as functions of H_1, H_2, and L are

$$\frac{H_2}{H_1} = -\frac{c(c+1)}{d(d+1)}, \tag{A 1.2}$$

$$\frac{\pi L}{H_1} = \frac{H_2}{H_1}\left\{\frac{c-d}{c(c+1)} - \log\left|\frac{1+c}{c}\right|\right\} - \log\left(\frac{1+d}{d}\right), \tag{A 1.3}$$

$$\frac{H_2}{\pi\Gamma} = c(c+1). \tag{A 1.4}$$

The equations for l_1 and l_2 in terms of c, d, and Γ are

$$\begin{aligned} &l_1(d-c)+d(d+1)\log(d-l_1) \\ &\quad -c(c+1)\log(l_1-c) = 1/\Gamma + d(d+1)\log d - c(c+1)\log|c| \end{aligned} \tag{A 1.5}$$

and

$$\begin{aligned} &l_2(d-c)+d(d+1)\log(d-l_2)-c(c+1)\log(c-l_2) \\ &\quad = 1/\Gamma + d(d+1)\log(d+1) - c(c+1)\log(c+1) + c - d. \end{aligned} \tag{A 1.6}$$

The quantities k_1, k_1', c, and d are related by

$$\begin{aligned} &k_1'(d-c)+d(d+1)\log(d-k_1')-c(c+1)\log(k_1'-c) \\ &\quad = k_1(d-c)+d(d+1)\log(d-k_1)-c(c+1)\log(k_1-c). \end{aligned} \tag{A 1.7}$$

L_1 is determined from the relation

$$L_1/\Gamma = k_1(d-c)+d(d+1)\log(1-k_1/d)-c(c+1)\log(1-k_1/c). \tag{A 1.8}$$

Similarly, for the second foil,

$$\begin{aligned} &k_2(d-c)+d(d+1)\log(d-k_2)-c(c+1)\log(k_2-c) \\ &\quad = k_2'(d-c)+d(d+1)\log(d-k_2')-c(c+1)\log(k_2'-c), \end{aligned} \tag{A 1.9}$$

and

$$L_2/\Gamma = L/\Gamma + (k_2'+1)(d-c)+d(d+1)\log\left(\frac{d-k_2'}{d+1}\right) - c(c+1)\log\left(\frac{k_2'-c}{c+1}\right). \tag{A 1.10}$$

In the calculations, c, d, Γ, l_1, and l_2 were first determined from the physical parameters, and then values of k_1 and k_2' were assumed as the further necessary input parameters. These 'mapped-cavity-length' parameters were used instead of the more natural physical-cavity lengths because of the high accuracy necessary in k_1 and k_2'. Thus a typical computation proceeded as follows:

(i) physical problem $\rightarrow H_1, H_2, L$;

(ii) $H_1, H_2, L \rightarrow c, d, \Gamma$;

(iii) $c, d, \Gamma \rightarrow l_1, l_2$;
(iv) k_1, k_2' assumed;
(v) $k_1, k_2' \rightarrow k_1', k_2, L_1, L_2$;
(vi) equations (14)–(17) $\rightarrow \sigma_1, \sigma_2, Q_1, Q_2$.

A typical set of parameter values is presented in table 1. It corresponds to a low-cavitation-number computation in the shallow staggered-foil case. The high accuracy needed for several of the parameters is to be noted.

z-plane	ζ-plane	Cavitation numbers and singularity strengths
$H_1 = 1{\cdot}0$	$k_2 = -1{\cdot}47223008$	$\sigma_1 = 0{\cdot}1$
$H_2 = 1{\cdot}0$	$l_2 = -1{\cdot}36085206$	$\sigma_2 = 0{\cdot}1$
$L_1 = 1{\cdot}8297862$	$k_2' = -0{\cdot}92612266$	$Q_1 = -0{\cdot}23735057$
$L_2 = 5{\cdot}9145975$	$c = -0{\cdot}92579977$	$Q_2 = 0{\cdot}30152621$
$L = 4{\cdot}5$	$k_1 = -0{\cdot}49548537$	
	$l_1 = -0{\cdot}31174158$	
	$k_1' = 0{\cdot}06445444$	
	$d = 0{\cdot}06453038$	

TABLE 1. Representative parameter values

Appendix 2. Expansion of $w(\zeta)$ for large ζ

After analytic continuation by reflexion about the real axis, the complex velocity $w(\zeta)$ (equation (12)) is regular outside the circle $|\zeta| = \max(|k_2|, k_1')$, and therefore has a Laurent expansion in the region outside that circle.

In this region, $H(\zeta)$ may be expanded in the form

$$-iH(\zeta) = \zeta^2 + h_1(l_1, l_2)\,\zeta + h_0(l_1, l_2) + \ldots \quad (|\zeta| > |l_2|), \tag{A 2.1}$$

where the explicit forms of $h_1(l_1, l_2), \ldots$, are not important. The pole at the leading edge of the upper foil is already in the desired form. The other pole may be expressed as

$$\frac{Q_2}{\zeta+1} = Q_2\left(\frac{1}{\zeta} - \frac{1}{\zeta^2} + \frac{1}{\zeta^3} - \ldots\right). \tag{A 2.2}$$

The $(\tau-\zeta)^{-1}$ term in each integrand in (12) is similarly expanded:

$$(\tau-\zeta)^{-1} = -\frac{1}{\zeta} - \frac{\tau}{\zeta^2} - \frac{\tau^2}{\zeta^3} - \ldots,$$

yielding integrals such as

$$I = \int_{k_2}^{l_2} \left(\frac{1}{\zeta\,|H(\tau)|} + \frac{\tau}{\zeta^2\,|H(\tau)|} + \frac{\tau^2}{\zeta^3\,|H(\tau)|} + \ldots\right) d\tau. \tag{A 2.3}$$

The integrand series in (A 2.3) is uniformly convergent in any closed subinterval of (k_2, l_2) that does not include either k_2 or l_2, and can thus be integrated term by term to give a series involving convergent improper integrals of the second kind (Apostol 1958):

$$I = \frac{1}{\zeta}\int_{k_2}^{l_2} \frac{d\tau}{|H(\tau)|} + \frac{1}{\zeta^2}\int_{k_2}^{l_2} \frac{\tau\,d\tau}{|H(\tau)|} + \frac{1}{\zeta^3}\int_{k_2}^{l_2} \frac{\tau^2 d\tau}{|H(\tau)|} + \ldots. \tag{A 2.4}$$

The expansion (A 2.2), the upper body pole, and the expansions typified by (A 2.4) are multiplied term by term with the expansion (A 2.1) of $H(\zeta)$, resulting in the (unique) Laurent expansion of the complex velocity for large ζ, which is given in (13).

Appendix 3. Elliptic integrals

Each of the coefficients in (14)–(17) can be expressed as a sum of complete and incomplete elliptic integrals (Byrd & Friedman 1954). A typical case is shown below.

$$\int_{k_2}^{l_2} \frac{d\tau}{(\tau-c)\{\tau(\tau-l_1)(\tau+1)(\tau-l_2)\}^{\frac{1}{2}}} = \frac{2}{(l_1-l_2)^{\frac{1}{2}}} \frac{1}{1+c} \times \left\{\frac{l_2+1}{l_2-c}\pi(\phi,\alpha^2,k) - F(\phi,k)\right\}, \quad \text{(A 3.1)}$$

where $$\phi = \sin^{-1}\left(\frac{l_2-k_2}{l_2(1+k_2)}\right)^{\frac{1}{2}}, \quad \alpha^2 = \frac{l_2(1+c)}{l_2-c}, \quad k^2 = \frac{l_2(1+l_1)}{l_2-l_1},$$

and $F(\phi,k)$ and $\pi(\phi,\alpha^2,k)$ are the incomplete elliptic integrals of the first and third kinds, respectively.

Appendix 4. Numerical evaluation of the lift coefficients

The numerical integrations indicated in (21) and (22) are straightforward, with the exception of the principal values in $K5$ and $J2$, and the singular behaviour of the inner integrals of $J1$, $J2$, $J3$, $K4$, $K5$, and $K6$. These cases are dealt with below.

(a) *Evaluation of the inner integrals of K5 and J2*

The inner integral of $K5$ may be written as

$$\int_{l_1}^{0} \frac{d\tau}{(\tau-\xi)\,|H(\tau)|} = \lim_{\delta\to 0}\left\{\int_{l_1}^{\xi-\delta} \frac{d\tau}{(\tau-\xi)\,|H(\tau)|} + \int_{\xi+\delta}^{0} \frac{d\tau}{(\tau-\xi)\,|H(\tau)|} + \int_{\xi-\delta}^{\xi+\delta} [F(\xi)/(\tau-\xi) + F'(\xi) + \tfrac{1}{2}F''(\xi)(\tau-\xi) + \tfrac{1}{6}F'''(\xi)(\tau-\xi)^2 + \ldots]\,d\tau\right\},$$

or $$\int_{l_1}^{0} \frac{d\tau}{(\tau-\xi)\,|H(\tau)|} = \int_{l_1}^{\xi-\delta} \frac{d\tau}{(\tau-\xi)\,|H(\tau)|} + \int_{\xi+\delta}^{0} \frac{d\tau}{(\tau-\xi)\,|H(\tau)|} + 2\delta F'(\xi) + \tfrac{1}{9}F'''(\xi)\,\delta^3 + O(\delta^5),$$

where $F(\xi) = |H^{-1}(\xi)|$; $\delta < \min\{|\xi-l_1|, \xi\}$. This expression may be written explicitly as

$$\int_{l_1}^{0} \frac{d\tau}{(\tau-\xi)\,|H(\tau)|} = \int_{l_1}^{\xi-\delta} \frac{d\tau}{(\tau-\xi)\,|H(\tau)|} + \int_{\xi+\delta}^{0} \frac{d\tau}{(\tau-\xi)\,|H(\tau)|} - \frac{\delta}{|H(\xi)|}\left(\frac{1}{\xi}+\frac{1}{\xi-l_1}+\frac{1}{\xi+1}+\frac{1}{\xi+l_2}\right)\left\{1+\frac{\delta^2}{18}\left(\frac{1}{\xi}+\frac{1}{\xi-l_1}+\frac{1}{\xi+1}+\frac{1}{\xi-l_2}\right)^{-1} M(\xi) + O\left(\frac{F^V(\xi)\delta^4}{600F'(\xi)}\right)\right\}, \quad \text{(A 4.1)}$$

where

$$M(\xi) = \frac{3}{2}\left(\frac{1}{\xi^2}+\frac{1}{(\xi-l_1)^2}+\frac{1}{(\xi+1)^2}+\frac{1}{(\xi-l_2)^2}\right)\left(\frac{1}{\xi}+\frac{1}{\xi-l_1}+\frac{1}{\xi+1}+\frac{1}{\xi-l_2}\right)$$
$$+2\left(\frac{1}{\xi^3}+\frac{1}{(\xi-l_1)^3}+\frac{1}{(\xi+1)^3}+\frac{1}{(\xi-l_2)^3}\right)+\frac{1}{4}\left(\frac{1}{\xi}+\frac{1}{\xi-l_1}+\frac{1}{\xi+1}+\frac{1}{\xi-l_2}\right)^3.$$

Using the same notation, the inner integral of $J2$ can be approximated by

$$\int_{-1}^{l_2}\frac{d\tau}{(\tau-\xi)\,|H(\xi)|} = \int_{-1}^{\xi+\epsilon}\frac{d\tau}{(\tau-\xi)\,|H(\xi)|}+\int_{\xi-\epsilon}^{l_2}\frac{d\tau}{(\tau-\xi)\,|H(\tau)|}$$
$$-\frac{\epsilon}{|H(\xi)|}\left(\frac{1}{\xi}+\frac{1}{\xi-l_1}+\frac{1}{\xi+1}+\frac{1}{\xi-l_2}\right)\left\{1+\frac{\epsilon^2}{18}\left(\frac{1}{\xi}+\frac{1}{\xi-l_1}+\frac{1}{\xi+1}+\frac{1}{\xi-l_2}\right)^{-1}M(\xi)\right.$$
$$\left.+O\left(\frac{F^V(\xi)\,\epsilon^4}{600F'(\xi)}\right)\right\}, \tag{A 4.2}$$

where $\epsilon < \min\{|\xi-l_2|, |\xi+1|\}$.

(*b*) *Limiting values of the outer integrands in* $J1$, $J2$, $J3$, $K4$, $K5$ and $K6$

The pertinent limiting values of the outer integrands in $J1$, $J2$, $J3$, $K4$, $K5$ and $K6$ are:

$$\left.\begin{aligned}
&(J1)\quad \lim_{\xi\to l_2(-)} G(\xi)\int_{k_2}^{l_2}\frac{d\tau}{(\tau-\xi)\,|H(\tau)|} = \frac{-\pi l_2(1+l_2)}{(l_2-c)\,(l_2-d)},\\
&(J2)\quad \lim_{\xi\to l_2(+)} G(\xi)\int_{l_2}^{-1}\frac{d\tau}{(\tau-\xi)\,|H(\tau)|} = 0,\\
&(J2)\quad \lim_{\xi\to -1(-)} G(\xi)\int_{l_2}^{-1}\frac{d\tau}{(\tau-\xi)\,|H(\tau)|} = 0,\\
&(J3)\quad \lim_{\xi\to -1(+)} G(\xi)\int_{-1}^{k_2'}\frac{d\tau}{(\tau-\xi)\,|H(\tau)|} = 0,\\
&(K4)\quad \lim_{\xi\to l_1(-)} G(\xi)\int_{k_1}^{l_1}\frac{d\tau}{(\tau-\xi)\,|H(\tau)|} = \frac{-\pi l_1(1+l_1)}{(l_1-c)\,(l_1-d)},\\
&(K5)\quad \lim_{\xi\to l_1(+)} G(\xi)\int_{l_1}^{0}\frac{d\tau}{(\tau-\xi)\,|H(\tau)|} = 0,\\
&(K5)\quad \lim_{\xi\to 0(-)} G(\xi)\int_{l_1}^{0}\frac{d\tau}{(\tau-\xi)\,|H(\tau)|} = 0,\\
&(K6)\quad \lim_{\xi\to 0(+)} G(\xi)\int_{0}^{k_1'}\frac{d\tau}{(\tau-\xi)\,|H(\tau)|} = 0,
\end{aligned}\right\} \tag{A 4.3}$$

where

$$G(\xi) = \frac{\xi(\xi+1)\,|H(\xi)|}{(\xi-c)\,(\xi-d)}.$$

REFERENCES

APOSTOL, T. M. 1958 *Mathematical Analysis.* Reading, Mass.: Addison-Wesley.

BIRKHOFF, G. & ZARANTONELLO, E. 1957 *Jets, Wakes, and Cavities.* New York: Academic Press.

BYRD, P. & FRIEDMAN, M. 1954 *Handbook of Elliptic Integrals for Engineers and Physicists.* Berlin: Springer-Verlag.

CHENG, H. K. & ROTT, N. 1954 Generalizations of the inversion formula of thin airfoil theory. *J. Rat. Mech. Anal.* **3**, 357–382.

DAWSON, T. E. & BATE, E. R. 1962 An experimental investigation of a fully cavitating two-dimensional flat plate hydrofoil near a free surface. *Karman Laboratory of Fluid Mechanics and Jet Propulsion Rep.* no. E-118.12, California Institute of Technology.

HSIEH, T. 1964 The linearized theory for a supercavitating biplane operating at zero cavitation number near a free surface. *Hydronautics, Inc. Tech. Rep.* no. 463–3, Laurel, Md.

PARKIN, B. R. 1959 Linearized theory of cavity flow in two dimensions. *RAND Corp. Rep.* no. P 1745, Santa Monica, Calif.

TULIN, M. P. 1953 Steady two-dimensional cavity flows about slender bodies. *DTMB Rep.* no. 834, Washington, D.C.

TULIN, M. P. 1964 Supercavitating flows—small perturbation theory. *J. Ship. Res.* **7**, 16–37.

VAN DYKE, M. D. 1964 *Perturbation Methods in Fluid Mechanics.* New York: Academic Press.

WETZEL, J. M. 1965 Tandem interference effects for noncavitating and supercavitating hydrofoils. *St Anthony Falls Hydr. Lab., Tech. Pap.* no. 50, series B, Minnesota.

YIM, B. 1964 On a fully cavitating two-dimensional flat plate hydrofoil with non-zero cavitation number near a free surface. *Hydronautics, Inc., Tech. Rep.* no. 463-4, Laurel, Md.